NASA Technical Memorandum 88827

Acousto-ultrasonic Verification of the Strength of Filament Wound Composite Material

Harold E. Kautz
Lewis Research Center
Cleveland, Ohio

Presented at the
Pressure Vessel Conference
sponsored by the American Society of Mechanical Engineers
Chicago, Illinois, July 21–24, 1986

NASA

ACOUSTO-ULTRASONIC VERIFICATION OF THE STRENGTH OF FILAMENT WOUND COMPOSITE MATERIAL

Harold E. Kautz
National Aeronautics and Space Administration
Lewis Research Center
Cleveland, Ohio 44135

SUMMARY

The concept of acousto-ultrasonic (AU) waveform partitioning was applied to nondestructive evaluation of mechanical properties in filament wound composites (FWC). A series of FWC test specimens were subjected to AU analysis and the results were compared with destructively measured interlaminar shear strengths (ISS). AU stress-wave factor (SWF) measurements gave greater than 90 percent correlation coefficient upon regression against the ISS. This high correlation was achieved by employing the appropriate time and frequency domain partitioning as dictated by wave propagation path analysis. There is indication that different SWF frequency partitions are sensitive to ISS at different depths below the surface.

INTRODUCTION

The acousto-ultrasonic approach has been described previously and shown to be a viable technique for characterizing mechanical strength properties of fiber reinforced composite laminates and filament wound composite structures (refs. 1 to 14). The approach depends on the introduction of ultrasonic waves and analysis of the resultant rather complex waveforms. These waveforms consist of the superposition of numerous multiple reflections of ultrasonic waves that interact with the material microstructure and boundary surfaces. The waveforms can be quantified in terms of a parameter called the stress wave factor (SWF).

The advent of digital waveform processing using the fast Fourier transform algorithm allows rapid analysis of frequency spectra. Frequency domain analysis has been successful in defining integrals and characteristic moments that exhibit sensitivity to properties of materials (ref. 15). At the same time, propagation path analysis has focused on identifying regions of the time domain associated with particular wave modes (ref. 16).

The SWF will correlate with properties such as tensile and interlaminar shear strength. For example, it has been shown that the SWF can be used to rank interlaminar shear strength of specimens cut from filament wound composite cylinders (ref. 17). To observe this relationship it was necessary to calculate SWF for a specific frequency band of the acousto-ultrasonic spectrum. The present work is an elaboration on this result and its theoretical foundations.

PROPAGATION PATH ANALYSIS

Although the ultimate application is to heterogeneous laminated or filament wound structures, it is useful to consider relatively simple monolithic media to model wave propagation paths. Analysis of the AU waveform can then proceed by partitioning according to particular wave propagation paths. This involves the identification of time and frequency domain regions that yield optimum correlations with material properties of interest.

Consider the transducer configuration shown in figure 1 where a sending transducer coupled to a solid introduces waves that reflect alternately off the back and front surfaces. Waves are represented by a ray construction approach where each ray is associated with a particular path from the sending to receiving transducer. Rays that are incident on the boundary surface at particular angles will, after some number j of reflections off the back surface in the medium, be intercepted by the receiving transducer. Rays are shown for $j = 1$, 2, and 3.

Figure 1 shows only the cases where all path segments represent longitudinal L waves. In fact, whenever a wave is reflected, even in isotropic monolithic media, two waves emerge, one L and one shear S wave. The L and the S waves emerge at different angles so the number of subsequent propagation paths increase with j.

Table I lists the 10 paths for $j = 1$ and 2. The calculations are made with reflection coefficient formulas from reference 18 and assuming L and S velocities and dimensions typical to the FWC bend specimens described in this report. The second column lists the sequence of modes for $j = 1$ and $j = 2$ paths. Table I lists all the permutations of L and S modes that start with an L wave leaving the sending transducer. The transit time column is of interest for identifying propagation paths in the time domain version of the AU signal. The cumulative reflection coefficient column lists the products of the multiple reflections at free surfaces for these paths. There is a reflection between each path segment. For a $j = 2$ path the cumulative reflection coefficient is the product of three reflections; two at the back surface and one at the front surface. A negative value for cumulative reflection coefficient represents a 180° phase shift.

If we replace the monolithic medium with a multilayered composite, additional internal reflections will arise and there will be more propagation paths to deal with, accompanied by exponential increases in mixed mode waves (refs. 19 and 20). The additional propagation paths will be those that reflect at interlaminar boundaries. The reflection coefficients for these will be sensitive to interlaminar properties. Therefore we expect that the SWF component from such a path will also be sensitive to the same properties.

The problem to be resolved by waveform partitioning is to extract useful information from the rather complex AU waveforms that arise due to the superposition of the above-mentioned paths. Propagation paths that undergo just one reflection should provide the least ambiguous information. Table I data can be used to bracket time domain regions of interest. This is illustrated in figure 2 where the simplest case, $j = 1$, for back surface reflection is presented along with two simple cases for internal reflections. (All ray paths in figure 2 are for L wave reflecting to L wave). Since the $j = 1$ back surface path in figure 2 has the greatest length waves traveling along the two

internal paths will get to the receiving transducer sooner. Thus the $j = 1$ path is an upper bound on the length of time for arrival of this type of internal reflections at the receiving transducer. This suggests that the early part of the AU signal, about the first 20 μs in the case of the specimens studied in this work, should, according to table I, give the least ambiguous information regarding internal structure.

EXPERIMENTAL PROCEDURE

Materials

Ten random samples were chosen from a large number of bend specimens cut from a segment of a FWC cylinder (ref. 17). The bend specimens were 12.7 by 1.27 by 0.64 cm parallelopipeds (fig. 3). The specimens were cut such that the width dimension, the 1.27 cm, was parallel to the curvature direction of the original FWC cylinder. This cylinder was on the order of 3 m in diameter. Thus the individual layers in the specimens exhibited negligible curvature and could be taken as consisting of flat and parallel planes.

Acousto-ultrasonic Measurements

AU measurements were made with a pair of 2.25 MHz center frequency transducers. Silicon rubber dry couplant pads were cemented to the 1.27 cm diameter wear plates of the transducers. The pads were 1.27 cm long, 0.3 cm wide, approximately 0.1 cm thick strips. The specimens were clamped between the transducers and a support base mounted on a jack with a force of 12 N (fig. 4).

AU signals arriving at the receiving transducer were amplified and digitized for computer processing. The energy of the signal was calculated and used as SWF. The energy is defined as the square of the amplified transducer output voltage integrated over the time of the sweep. Thirteen overlapping measurements were taken at 0.64 cm intervals along the length of the specimens. The transducers centerline separation was 3.8 cm.

AU waveforms were collected at each of 13 overlapping positions on each side of all the specimens. Three waveforms were collected at each position on all 10 specimens so that a total of 780 waveforms were collected and stored on disc. Once this was accomplished the specimens were available for three point bend testing.

Mechanical Testing

The bend tests were performed by the three point contact method in a standard tensile test machine. The stress-strain records were used to calculate three mechanical properties as follows (ASTM standards, ref. 21). For interlaminar shear strength

$$ISS = \frac{3P}{4bd},$$

For ultimate flexure strength

$$UFS = \frac{3PL}{2bd^2},$$

and for the tangent modulus of elasticity

$$TME = \frac{L^3 s}{4bd^3},$$

where P = maximum load in newtons, N; b = width of specimen in meters, m; d = thickness of specimen at midspan, m; L = support span, m, (L = 0.1016 m for all specimens); and s = slope of tangent of stress-strain record at initial straight line portion of load-deflection curve, N/m.

Figure 5 is a typical stress-strain record obtained in the three point bend tests. All specimens were stressed to failure as defined by reaching the region marked C where they had clearly lost the bulk of their strength. As with the case of reference 17 the ISS and UFS were calculated using the value of the stress at point A, the first break in the curve as maximum load P. Also as with reference 17, the point B, the highest stress recorded, was also used as maximum load. But point B data always gave lower correlation with AU data. Only point A data is quoted in this report.

The raw bend test data were stored on disc. Orientation of bend tests relative to acousto-ultrasonic SWF measurements is shown in figure 6. Measurements at position 7, both on the concave and the convex side, were centered on the plane of maximum stress through the thickness of the specimen during the bend experiment.

RESULTS AND ANALYSIS

Figure 7(a) is a typical frequency spectrum obtained for the FWC bend specimens. The spectrum usually peaked in the vicinity of 0.6 to 0.7 MHz. The waveforms were digitized with conditions that result in a Nyquist frequency of 1.28 MHz. Figure 7(b) is a spectrum taken of the same specimen and transducers but with conditions that result in a Nyquist frequency of 5.12 MHz. Although there are some spectral components out to about 2.25 MHz, the major portion is still between 0.6 to 0.7 MHz. Figure 7(a) conditions were used in the experiment because they permit examination of the full time domain of the AU signal while conditions corresponding to figure 7(b) allow only partial examination.

Table II lists the mean densities and mechanical data obtained for the specimens in the three point bend tests. Each of these were regressed against SWF in the various time and frequency domain partitioning schemes to be described.

Figure 8 introduces the AU waveform partitioning method used to compare correlation results between the SWF and mechanical test results. The format of figure 8 will be used to present correlation coefficients, R, for regression of partitioned SWF against ISS. It depicts a partitioning scheme for the time and frequency domains of the AU signal. The 200 μs time window was divided into ten 20 μs partitions. The 1.28 MHz frequency domain was divided

into four 0.32 MHz partitions. The largest section in figure 8 is for SWF's that involve partitioning of both the time and frequency domains. For example, the block marked "A" in figure 8 pertains to R value calculated from the SWF of the total waveforms. The block "B" is for the R value of the 0 to 0.32 MHz band of the total time domain signal. Conversely, the strip along the bottom is for time partitioning with the total frequency spectrum. The example block "C" is for the total spectrum of the time interval 120 to 140 μs. The largest group of blocks is for two-dimensional partitioning. The example block "D" is for R value calculated with the SWF of the 0.32 to 0.64 MHz strip of the 40 to 60 μs portion of the waveform.

Figure 9 is a representative graph of the partitioned SWF versus ISS for the 10 specimens of this experiment. SWF is an increasing function of ISS but it is not linear. If, however, the two specimens with lowest SWF and ISS are excluded the other eight suggest a straight line. Figure 9 shows that SWF is an increasing function of ISS over the range spanned by all 10 specimens. However it was a further purpose of these experiments to identify time and frequency partitions of SWF that show the highest sensitivity to ISS. For this reason only the eight specimens in the linear regime of figure 9 were used for the results presented in the rest of this report. Linear regression of SWF versus ISS was performed and the correlation coefficient used as the measure of the sensitivity.

Correlation coefficients, R, for partitioned SWF and ISS are presented in the format of figure 8 in figures that follow. These figures are in three parts. Part (a) lists the values of R. Parts (b) and (c) are bar graphs, in the same format, of these R values. Part (b) shows R in the range 0.50 to 1.00 and part (c) shows R from 0.75 to 1.00.

While each regression coefficient figure employs data from the complete set of eight specimens, it pertains to a particular position on the specimens. Only data from position 7 is presented in these figures. Position 7, on both the convex and concave sides, is at the midpoint load pin and hence at the expected maximum stress yield point in the three point bend test.

The partition scheme presented in figure 10, for AU data collected on the convex side of the specimens, contains frequency partitions chosen to match those reported in reference 17. These partitions are: the total time and frequency domain, as well as total time with frequency partitions up to 1.024 MHz. (The filter 1.024 to 1.28 MHz was above the Nyquist frequency in reference 17 and therefore was not available.) THe partitions that are identical with those in reference 17 can be compared. The partition: 0.512 to 0.768 MHz - total time domain has the highest correlation coefficient in the group just as in reference 17.

The highest among all the correlation coefficients in figure 10 is 0.92 for the partition: 1.024 to 1.28 MHz - total time domain. Figure 10 also exhibits some high coefficients in the early time partitions.

Slightly different frequency partitions were used in figure 11 than in figure 10 for the same AU data. They are shifted towards higher frequencies by making each 0.32 MHz wide rather than 0.256. The highest R is 0.93 for the partition: 0 to 20 μs with 0.64 to 0.96 MHz. Again the early time partitions, particularly 0 to 20 μsec, show the best correlations of SWF with ISS. High correlations of the total time domain listed in the strip at the

right in figure 11 reflect the fact that the total time domain is dominated by its early portions. Figure 12 is a plot of SWF versus ISS, with the data of this highest R partition in figure 11.

In figure 13 the partition scheme of figure 11 is applied to the AU data taken on the opposite sides of the specimens. The best correlation is in the partition: 0 to 20 μs with 0.32 to 0.64 MHz. This side of the specimens is that which is concave after the bend test and is the farther from the yield point. In reference 17 no correlation was detected on this side. In the present work time partitioning has revealed several partitions with at least moderate correlation.

Each of the partition schemes presented thus far includes ten 20 μs wide, time partitions. Schemes with 10 μsec width were also tried but showed low correlation. However it seemed desirable to examine the 0 to 20 μs time range in greater detail because of the generally high R values found there. As an alternative to narrower partitions, overlapping 20 μs partitions were calculated. This data is presented in figures 14 and 15. Figure 14 is for the convex side of the specimens and figure 15 is for the concave side. The results are as expected from the 0 to 20 μsec columns of figures 11 and 13. That is, the convex side data shows highest correlations for 0.64 to 0.96 MHz and the concave side data is best for 0.32 to 0.64 and for 0.96 to 1.28 MHz.

Figure 16 presents the data from the set of conditions that gave the highest correlation for all calculations in these experiments. This was achieved on the concave side of the specimen in the partition: 6 to 26 μs with 0.96 to 1.28 MHz. This data, with R = 0.97, is quite linear and it was evident that the two excluded specimens were not of the same population.

Many other positions on the specimens, other than center position number 7, and a wide range of averages over positions were calculated but no correlations greater than about 0.70 were obtained. SWF measured at the midpoint position 7 of greatest stress always gave the best correlation with ISS. At positions 6 and 8 which were only 0.64 cm away the SWF did not correlate with ISS.

The left side of figure 17 shows SWF position profiles of four of the specimens of figure 16. These four were chosen to show the range of profiles existing among the specimens. A symbol marks position 7 for each of the four. On the right side of figure 17 the symbols plot the position 7 SWF versus ISS. In some cases SWF at position 7 is much greater than at either 6 or 8. Since ISS correlates with R = 0.97 in this partition we assume that ISS has a very similar profile. Thus these specimens are weaker to interlaminar shear at position 6 or 8 than at 7. Even though the stress is greater at 7 at any given time during the test, still position 6 or 8 might see their limit first. In this case the SWF at position 7 would not be the one sensitive to ISS. To test this, SWF chosen from the lowest among positions 6, 7, and 8 was regressed against ISS, but correlation coefficients were lower than with position 7 alone. This result indicates that the three point bend test gives ISS results that are quite specific to the center pin position.

Test correlations were tried between SWF and calculated ultimate tensile strength and also with tangent modulus of elasticity. As expected, reference 17, no significant correlation could be found.

DISCUSSION

This work demonstrates the value of time and frequency domain partitioning of acousto-ultrasonic (AU) waveforms for the purpose of revealing the relation between stress-wave factor (SWF) and interlaminar shear strength (ISS) of graphite-epoxy filament wound composite material.

The partition schemes were compared by regression analysis based upon the linear portion of the SWF versus ISS relation found in the data. This was for large ISS values. ISS drops rapidly from the line below some threshold value of about 8.5×10^6 MPa. These partitions were best compared using the eight specimens that had ISS value above the threshold. It should be noted that, although the two specimens that were excluded do not fall near the regression curves, their SWF's are, overall, part of the same increasing function of ISS as the others.

The regression curve intercepts the ISS axis at a positive value. This implies that there is a residual ISS when SWF is zero. Assume that there are N interlaminar boundaries in the specimen. The SWF measures ISS at the boundary j of failure, where $1 < j < N$. In the limit of zero strength in boundary j the SWF is also zero. The three point bend test, however, still measures the residual strength residing in the other n-1 boundaries. The two specimens that do not fit the regression curve may be exceptionally weak throughout their thickness, which includes the residual strength regions.

As predicted by analysis of ray paths, the strong sensitivity of SWF to ISS is in the first 20 μs of the time domain signal. The results revealed the need to more finely partition the first 20 μs of the time domain. The present data was not amenable to this. Ten microsecond partition widths produced SWF values that were subject to the wave oscillations. Since the spectrum peaks in the range of 0.6 to 0.7 MHz, 10 μs of the time domain is only about six oscillations of the dominant frequency. Finer partitioning may be possible by employing higher frequency transducers and shorter time domains.

On the other hand, application of this technique to thicker specimens may resolve the problem in the opposite direction. That is, a specimen that is thicker than the present bend specimens would have a similarly sensitive time domain beyond 20 μs.

The frequency dependence observed cannot be explained by propagation path analysis. The SWF measured on the concave side of the specimens correlated with ISS in different frequency ranges than in the case of the convex sides. The difference between convex, (fig. 14), and concave, (fig. 15), to SWF measurements is depth at which the interlaminar shear occurred. The region that sheared during the bend test was deeper on the concave side. This suggests the possibility that frequency filtering might be useful to separate the sensitivity of different depths from the surface.

The SWF was found to be related to the ISS at the position on the specimen that was within ± 0.64 cm of the midpoint between the sending and receiving transducer. This localization suggests that two-dimensional AU scanning can be utlilized to produce two-dimensional ISS profiles. If the dependence of sensitivity depth on frequency can be developed, three-dimensional mapping of ISS in graphite/epoxy materials may be possible.

CONCLUSIONS

These experiments demonstrate that stress wave factor (SWF), determined from acousto-ultrasonic (AU) data, is a sensitive indicator of interlaminar shear strength (ISS) in graphite/epoxy filament wound composite (FWC) materials. The correlation between SWF and ISS can be optimized by appropriate partitioning of the AU signal.

Time domain partitioning reveals that portions of the AU signal that are dominated by arrival at the receiving transducer of simple, one reflection, ray paths contain the most precise information about ISS at the position of the reflection.

Frequency domain partitioning suggests that different portions of the frequency spectrum are sensitive to ISS at different depths below the surface where the ultrasonic energy is introduced and detected.

The SWF was found to be related to the ISS at the position on the specimen that was within $\pm$0.64 cm of the midpoint between the sending and the receiving transducer.

REFERENCES

1. Vary, A., and Bowles, K.F., "Ultrasonic Evaluation of the Strength of Unidirectional Graphite Polymide Composites," Proceedings of the Eleventh Symposium on Nondestructive Testing, ASNT, San Antonio, TX, 1977, pp. 242-258.

2. Hayford, D.T., Henneke, E.G., II, and Stinchcomb, W.W., "The Correlation of Ultrasonic Attenuation and Shear Strength in Graphite-Polymide Composites," Journal of Composite Materials, Vol. 11, Oct. 1977, pp. 429-444.

3. Vary, A., and Bowles, K.J., "Use of an Ultrasonic-Acoustic Technique for Nondestructive Evaluation of Fiber Composite Strength," Reinforced Plastics - Contact 78, Proceedings of the 33rd Annual Conference, SPI, New York, 1978, Section 24-A, pp. 1-5.

4. Vary, A., and Lark, R.F., "Correlation of Fiber Composite Tensile Strength with the Ultrasonic Stress Wave Factor," Journal of Testing and Evaluation, Vol. 7, No. 4, July 1979, pp. 185-191.

5. Williams, J.H., Jr., and Doll, B., "Ultrasonic Attenuation as an Indicator of Fatigue Life of Graphite Fiber Epoxy Composite," Materials Evaluation, Vol. 38, No. 5, May 1980, pp. 33-37.

6. Williams, J.H., Jr., Nayeb-Hashemi, H., and Lee, S.S., "Ultrasonic Attenuation and Velocity in AS/3501-6 Graphite Fiber Composite," Journal of Non-Destructive Evaluation, Vol. 1, No. 2, June 1980, pp. 137-148.

7. Williams, J.H., Jr., and Lampert, N.R., "Ultrasonic Evaluation of Impact-Damaged Graphite Fiber Composite," Materials Evaluation, Vol. 38, No. 12, Dec. 1980, pp. 68-72.

8. Schramm, S.W., Daniel, I.M., and Hamilton, W.G., "Evaluation of Sensitivity of Ultrasonic Detection of Disbonds in Graphite/Epoxy to Metal Joints," Working Together for Strength, Preprint of the 36th Annual Conference, Reinforced Plastics/Composites Institute. Society of the Plastics Industry, New York, 1981, Session 23-D, pp. 1-6.

9. Williams, J.H., Jr., Yuce, H., and Lee, S.S., "Ultrasonic and Mechanical Characterizations of Fatigue States of Graphite Epoxy Composite Laminates," Materials Evaluation, Vol. 40, No. 5, Apr. 1982, pp. 560-565.

10. Henneke, E.G., II, Duke, J.C., Jr., Stinchcomb, W.W., Govada, Anil, and Lemascon, A., "A Study of the Stress Wave Factor Technique for the Characterization of Composite Materials," NASA CR-3670, 1983.

11. Hemann, J.H., and Baaklini, G.Y., "The Effect of Stress on Ultrasonic Pulses in Fiber Reinforced Composites," NASA CR-3724, 1983.

12. Wehrenberg, R.H., II, "New NDE Technique Finds Subtle Defects," Materials Engineering, Vol. 92, No. 3, Sept. 1980, pp. 59-63.

13. Serabian, S., "Composite Characterization Techniques: Ultrasonic," Mantech Journal, Vol. 10, No. 3, 1985, pp. 11-23.

14. Lorenzo, L., and Hahn, H.T., "Damage Assessment by Acousto-Ultrasonic Technique in Composites," WU/CCR-86/2, Washington University, St. Louis, MO, Apr. 1986.

15. Govada, A., Henneke, E.G., II, and Talreja, R., "Acousto-Ultrasonic Measurements to Monitor Damage During Fatigue of Composites," 1984 Advances in Aerospace Sciences and Engineering, U. Yuceoglu and R. Hesser, eds., ASME, New York, 1984, pp. 55-60.

16. Karagulle, H., Williams, J.H., and Lee, S.S., "Stress Waves in an Isotropic Elastic Plate Excited by a Circular Transducer," NASA CR-3877, 1985.

17. Kautz, H.E., "Ultrasonic Evaluation of Mechanical Properties of Thick, Multilayered, Filament Wound Composites," NASA TM-87088, 1985.

18. Krautkramer, J., and Krautkramer, H., Ultrasonic Testing of Materials. Springer-Verlag, New York, 1969, pp. 476-481. (Translation of second revised German edition, by B.W. Zenzinger).

19. Green, R.E., Jr., "Ultrasonic Nondestructive Materials Characterization," Analytical Ultrasonics in Materials Research and Testing, A. Vary, ed., NASA CP-2383, 1984, pp. 1-29.

20. Henneke, E.G., and Duke, J.C., "Analytical Ultrasonics for Evaluation of Composite Materials Response, Part I: Physical Interpretation," Analytical Ultrasonics in Materials Research and Testing Conference, NASA CP-2383, 1986, pp. 141-152.

21. 1986 Annual Book of ASTM Standards. ASTM D790-84a, "Flexural Properties of Unreinforced and Reinforced Plastics and Electrical Insulating Materials." ASTM D2344-84, "Apparent Interlaminar Shear Strength of Parallel Fiber Composites by Short-Beam Method."

TABLE I. - CALCULATED TRANSIT TIME, T, AND CUMULATIVE REFLECTION COEFFICIENT, R FOR MULTIPLE REFLECTIONS IN A MONOLITHIC MEDIUM

Reflection order, j[a]	Wave-mode sequence[b]	Transit time, T μs[c]	Cumulative reflection coefficient, R[c]
1	L-L	15.01	-0.319
1	L-S	18.49	.288
2	L-L-L-L	16.93	-.041
2	L-L-L-S	19.76	.046
2	L-L-S-L	19.76	.276
2	L-S-L-L	19.76	.276
2	L-L-S-S	22.76	.039
2	L-S-L-S	22.76	-.414
2	L-S-S-L	22.76	.268
2	L-S-S-S	26.02	.052

[a] j = number of back surface reflections.
[b] L = longitudinal wave path segment, S = shear wave path segment.
[c] Calculated with transducer separation = 3.8 cm, thickness = 0.63 cm, longitudinal velocity = 0.27 cm/μs and shear velocity = 0.14 cm/μs.

TABLE II. - MECHANICAL DATA FOR BEND SPECIMENS

Specimen designation	Density, g/cm^3	Interlaminar shear strength, MPa	Ultimate tensile strength, MPa	Tensile modulus of elasticity, MPa
B31	1.50106	9.31399E+06	2.74952E+08	1.17962E+10
23	1.44902	8.76399E+06	2.89719E+08	1.52020E+10
A22	1.48646	9.39139E+06	2.82448E+08	1.24289E+10
22	1.44831	7.36706E+06	2.36693E+08	1.19386E+10
34	1.37299	3.62416E+06	1.11580E+08	1.01516E+10
A32	1.50243	9.65676E+06	2.92629E+08	1.32961E+10
12	1.43574	9.26278E+06	2.85009E+08	1.15598E+10
A31	1.53824	9.63898E+06	2.92090E+08	1.41620E+10
B21	1.51063	8.80280E+06	2.67766E+08	1.25898E+10
A21	1.53824	9.09895E+06	2.75726E+08	1.41620E+10

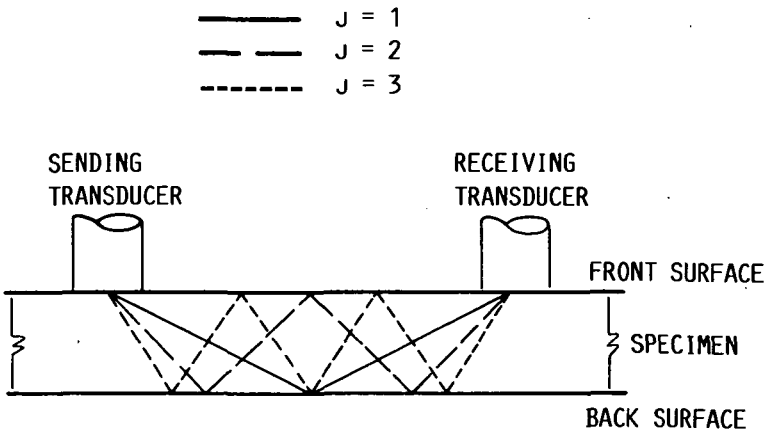

FIGURE 1. - RAY PATHS FOR SIMPLE BACK SURFACE AND FRONT SURFACE REFLECTION LONGITUDINAL WAVE PROPAGATION MODE IN MONOLITHIC MEDIUM.

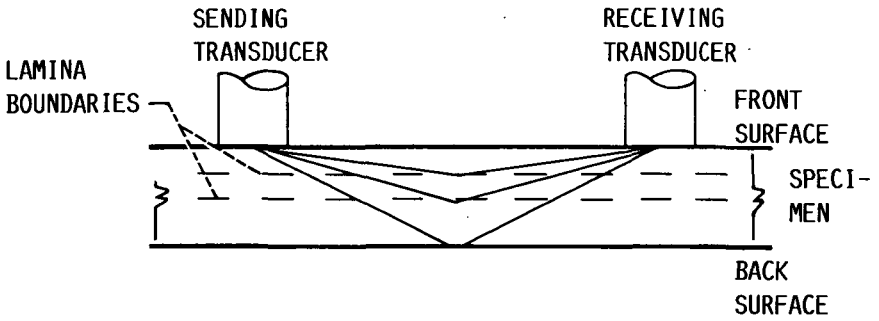

FIGURE 2. - RAY PATHS FOR LAMINATED MEDIUM SHOWING J = 1 BACK SURFACE REFLECTION AND TWO SIMILAR INTERNAL REFLECTIONS.

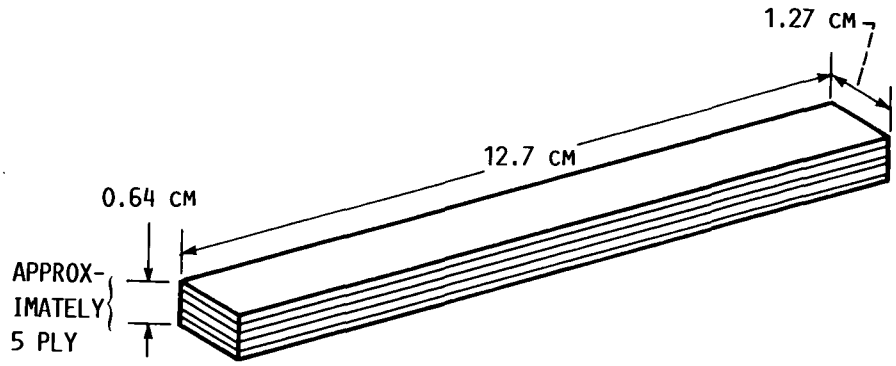

FIGURE 3. - TYPICAL BEND SPECIMEN.

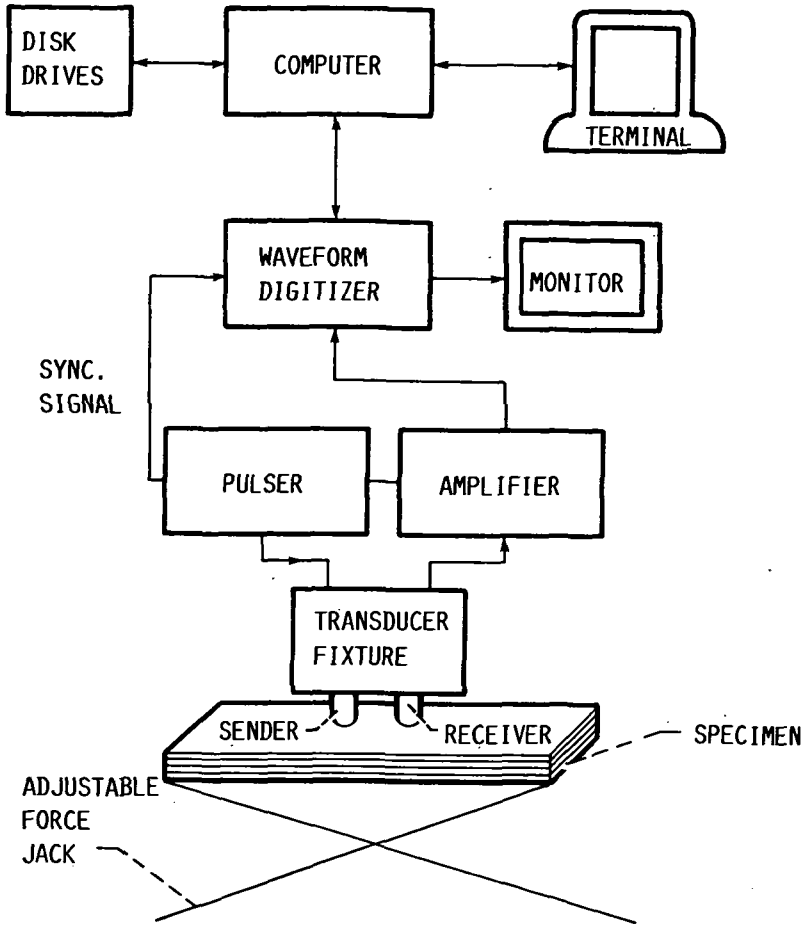

FIGURE 4. - BLOCK DIAGRAM OF ACOUSTO-ULTRASONIC AND DATA PROCESSING SYSTEM.

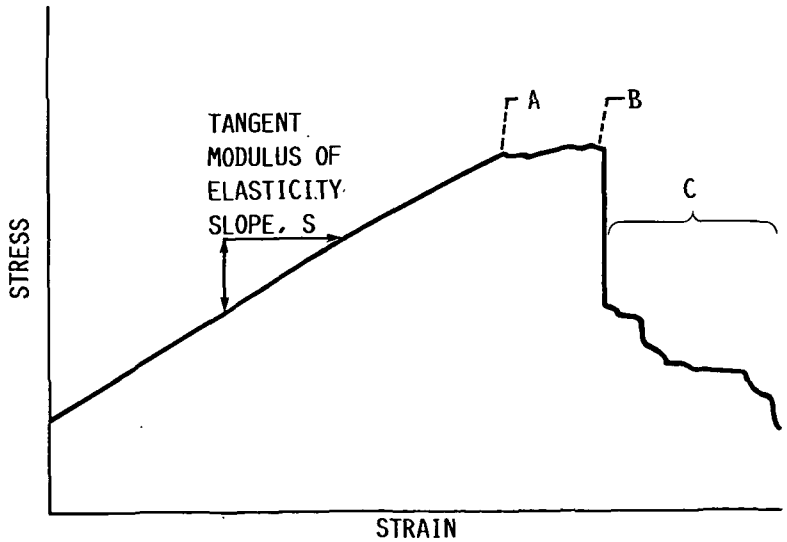

FIGURE 5. - TYPICAL STRESS-STRAIN CURVE FROM THREE POINT BEND TEST OF FWC SPECIMEN. A IS FIRST BREAK IN CURVE. B IS MAXIMUM OF CURVE. C IS REGION BEYOND FAILURE.

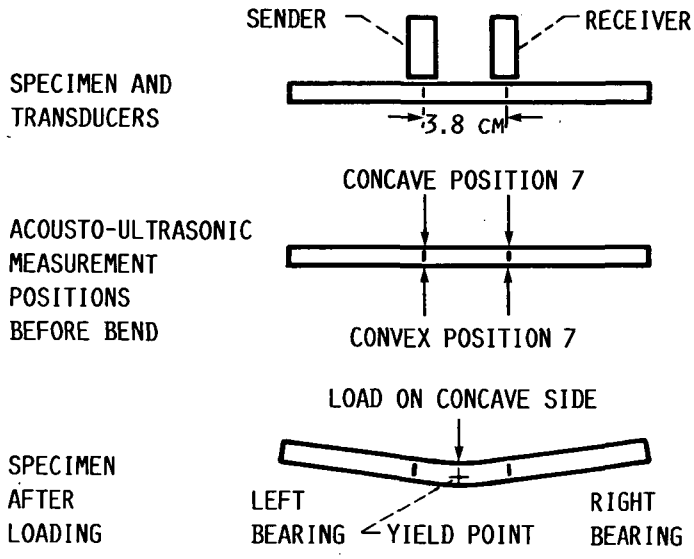

FIGURE 6. - DIAGRAM OF BEND TEST SPECIMEN ILLUSTRATING RELATIVE ORIENTATION OF ACOUSTO-ULTRASONIC MEASUREMENTS AND BEND TEST SUPPORT POINTS. ACOUSTO-ULTRASONIC MEASUREMENTS WERE MADE ON BOTH CONCAVE AND CONVEX SIDES AT 13 OVERLAPPING POSITIONS FROM LEFT END TO RIGHT END.

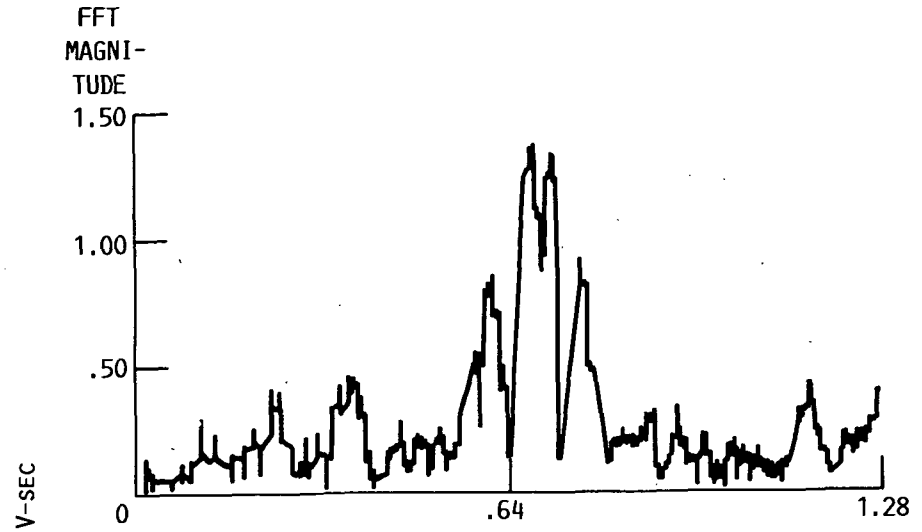

(A) NYQUIST F = 1.28 MHz.

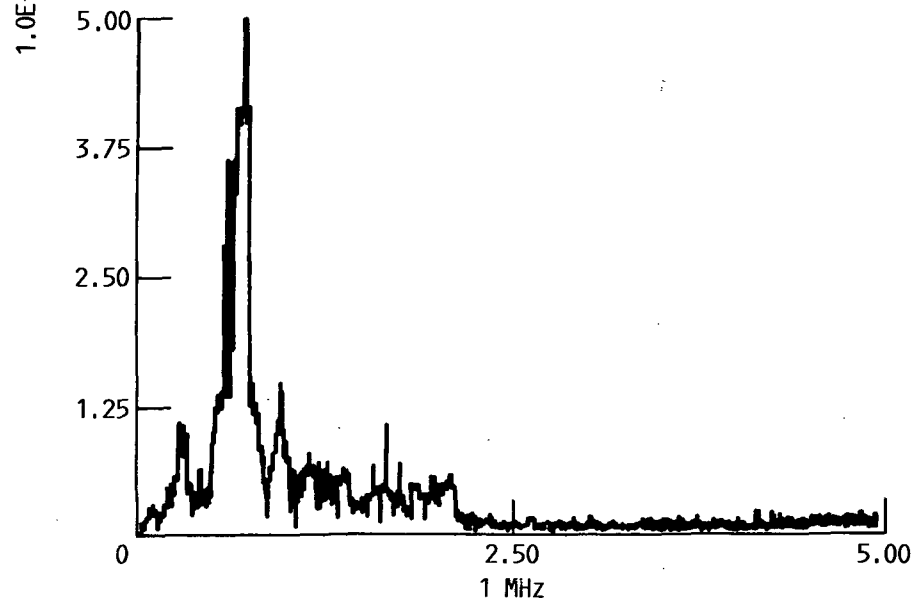

(B) NYQUIST F = 5.12 MHz.

FIGURE 7. - FREQUENCY SPECTRUMS FROM DIGITIZED SIGNALS COLLECTED ON FWC BEND SPECIMENS.

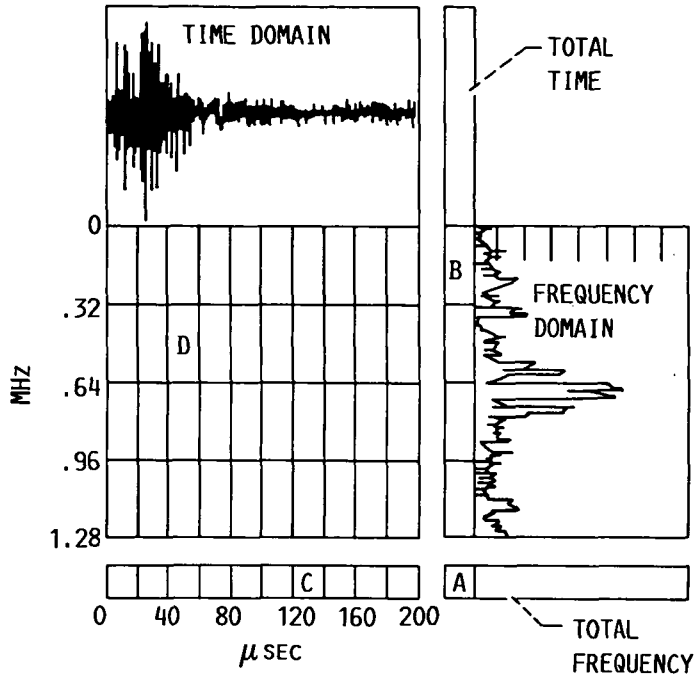

FIGURE 8. - ILLUSTRATION OF ONE 2-DIMENSIONAL WAVEFORM PARTITIONING SCHEME FOR SWF CALCULATIONS AND FORMAT FOR PRESENTING REGRESSION COEFFICIENTS IN SUBSEQUENT FIGURES.

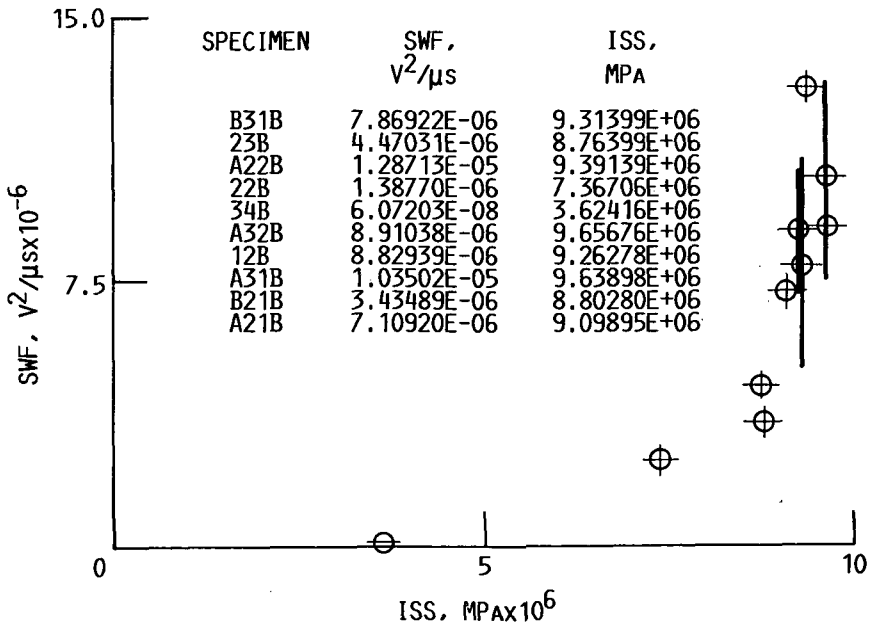

FIGURE 9. - STRESS WAVE FACTOR VERSUS INTERLAMINAR SHEAR STRENGTH. SPECIMENS: ALL 10. POSITION: 7, CONVEX SIDE. PARTITION: TOTAL FREQUENCY, 0 TO 1.28 MHZ AND 0 TO 20 MICROSECONDS.

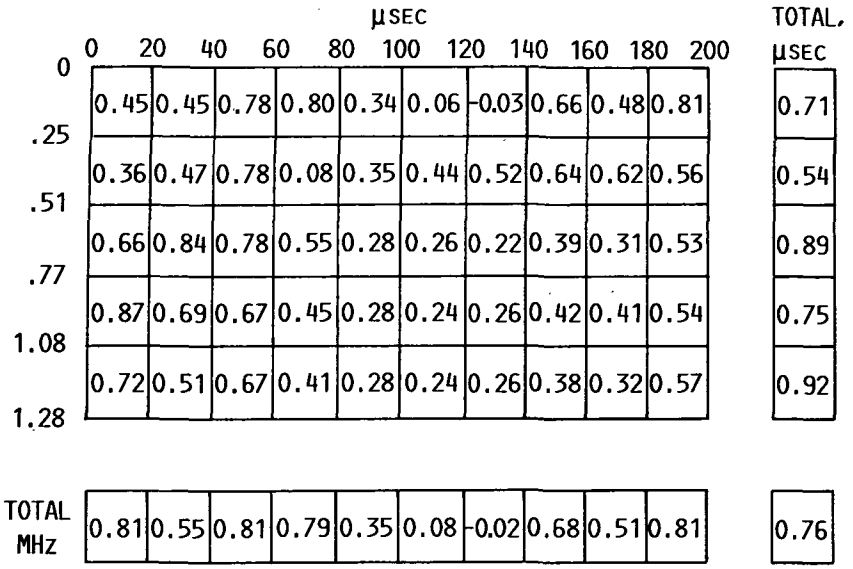

(A) VALUE OF R.

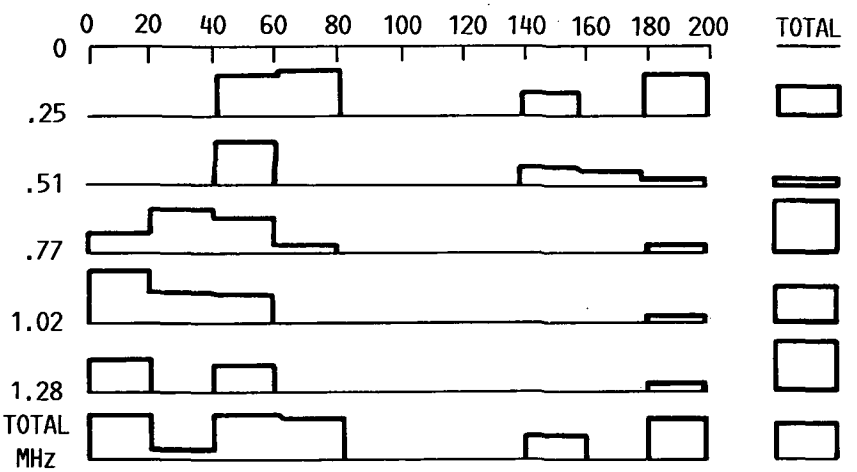

(B) BAR GRAPH R = 0.50 TO 1.00.

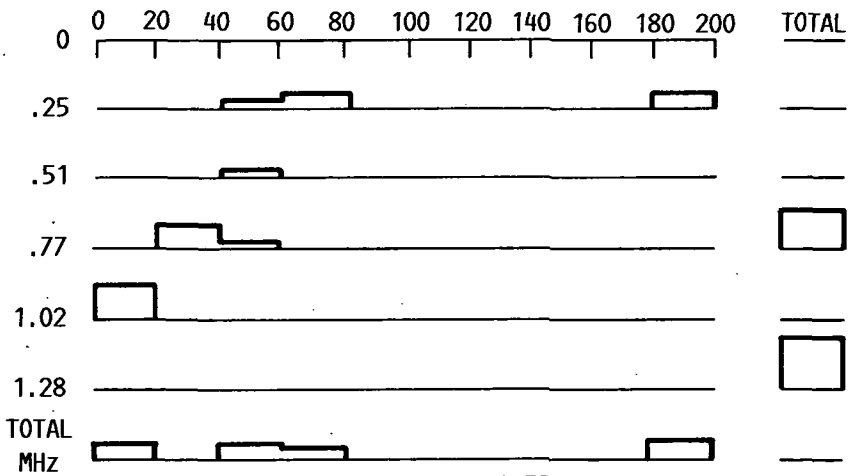

(C) BAR GRAPH R = 0.75 TO 1.00.

FIGURE 10. - LINEAR REGRESSION COEFFICIENTS FOR PARTITIONED STRESS WAVE FACTOR VERSUS INTERLAMINAR SHEAR STRENGTH. SPECIMENS INCLUDED: 8 SELECTED. POSITION OF SWF MEASUREMENT: NO. 7, CONVEX SIDE.

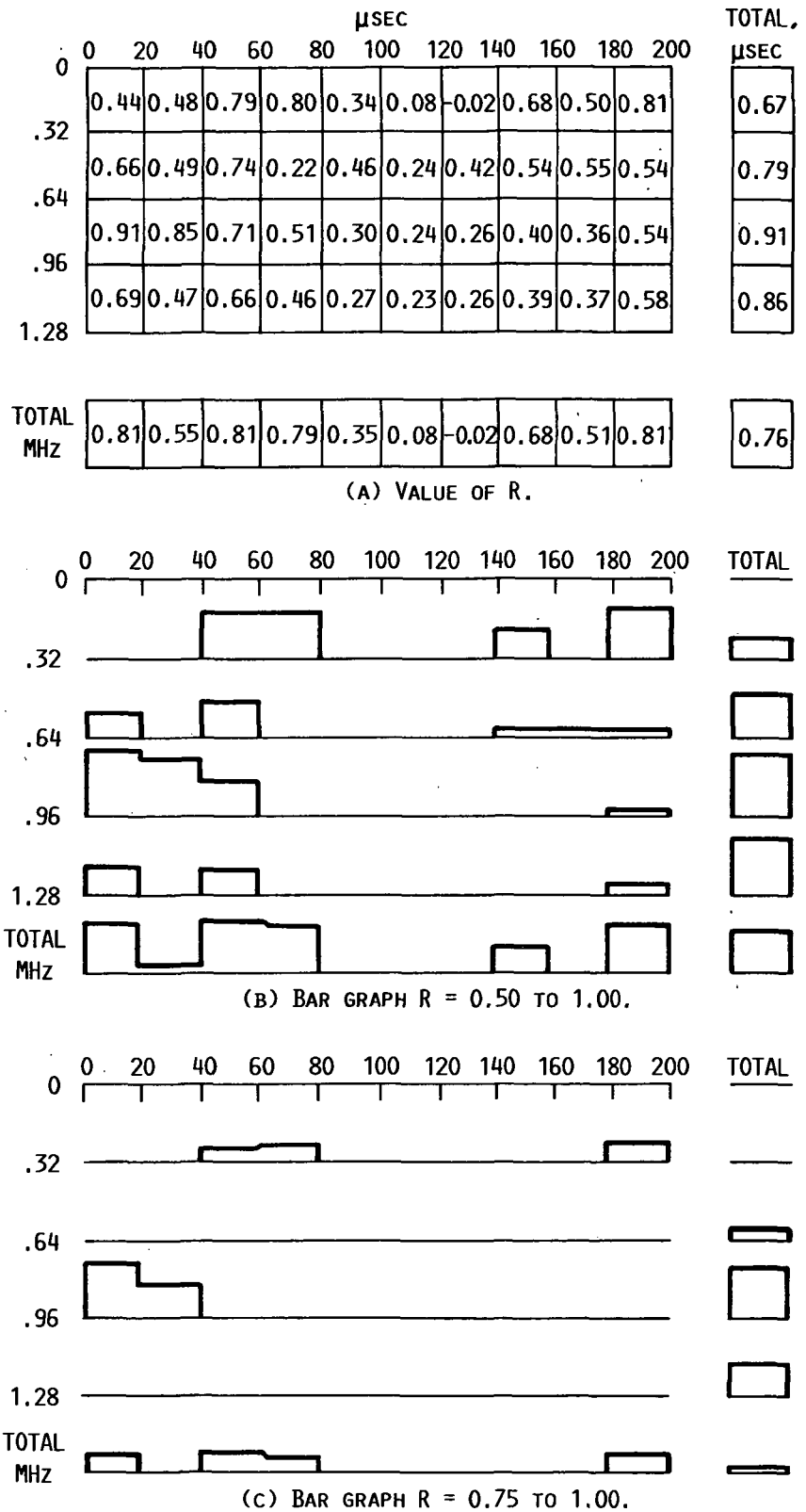

FIGURE 11. - LINEAR REGRESSION COEFFICIENTS FOR PARTITIONED STRESS WAVE FACTOR VERSUS INTERLAMINAR SHEAR STRENGTH. SPECIMENS INCLUDED: 8 SELECTED. POSITION OF SWF MEASUREMENT: NO. 7, CONVEX SIDE.

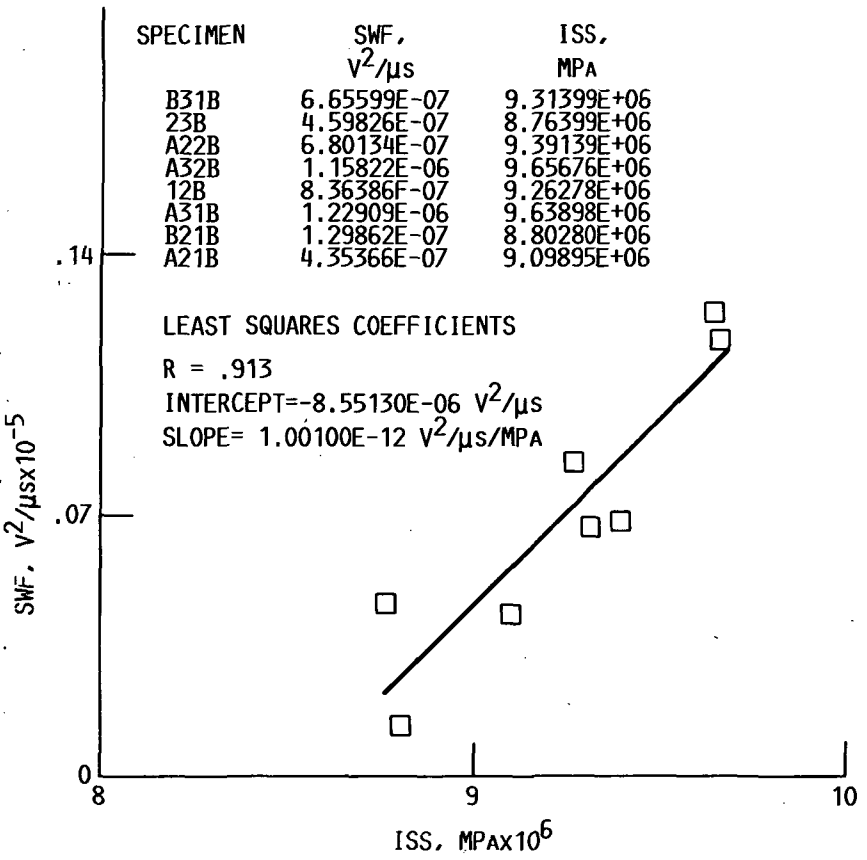

FIGURE 12. - STRESS WAVE FACTOR VERSUS INTERLAMINAR SHEAR STRENGTH WITH LINEAR REGRESSION CURVE. POSITION: 7, CONVEX SIDE. PARTITION: 0.64 TO 0.96 MHZ AND 0 TO 20 MICROSECONDS.

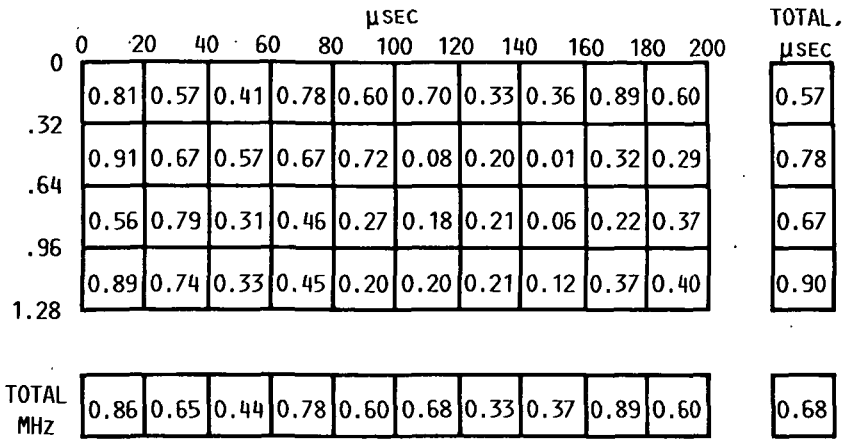

(A) VALUE OF R.

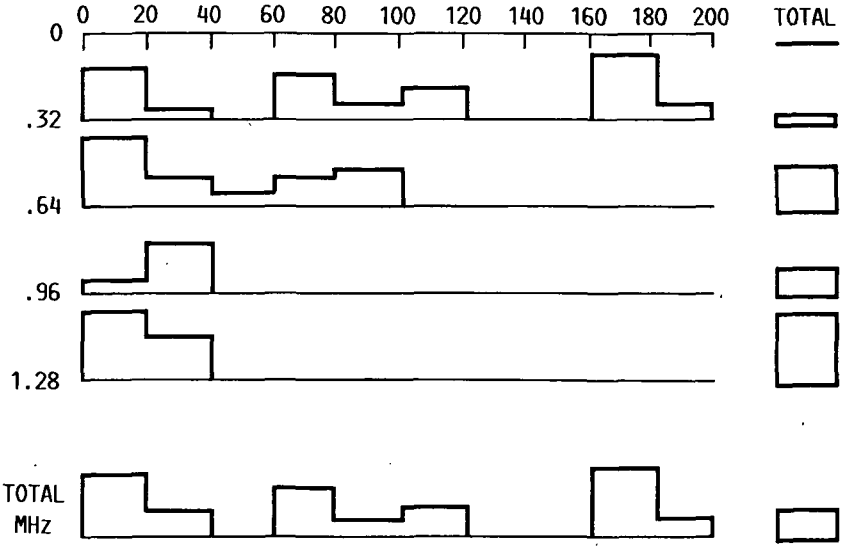

(B) BAR GRAPH R = 0.50 TO 1.00.

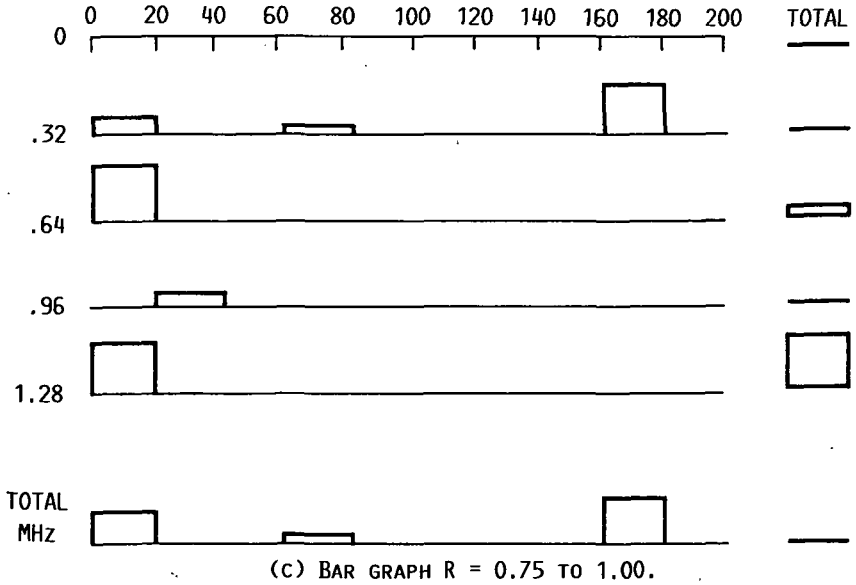

(C) BAR GRAPH R = 0.75 TO 1.00.

FIGURE 13. - LINEAR REGRESSION COEFFICIENTS FOR PARTITIONED STRESS WAVE FACTOR VERSUS INTERLAMINAR SHEAR STRENGTH. SPECIMENS INCLUDED: 8 SELECTED. POSITION OF SWF MEASUREMENT: NO. 7, CONCAVE SIDE.

20 μSEC PARTITION WIDTH STARTING AT:

	0	1	2	3	4	5	6	7	8	9	10	11	12	13	14	15	16	μSEC
0	0.40	0.37	0.35	0.26	0.26	0.21	0.10	0.33	0.37	0.37	0.35	0.32	0.53	0.53	0.51	0.54	0.51	
.32	0.70	0.63	0.61	0.50	0.54	0.58	0.64	0.66	0.51	0.55	0.60	0.66	0.69	0.55	0.55	0.56	0.46	
.64	0.91	0.92	0.95	0.93	0.95	0.92	0.91	0.92	0.87	0.89	0.90	0.91	0.89	0.91	0.90	0.90	0.84	
.96	0.74	0.85	0.89	0.83	0.90	0.93	0.93	0.88	0.94	0.86	0.87	0.92	0.91	0.74	0.81	0.66	0.63	
1.28																		
TOTAL MHz	0.80	0.77	0.76	0.56	0.59	0.56	0.49	0.67	0.66	0.67	0.65	0.63	0.70	0.65	0.63	0.62	0.58	

(A) VALUE OF R.

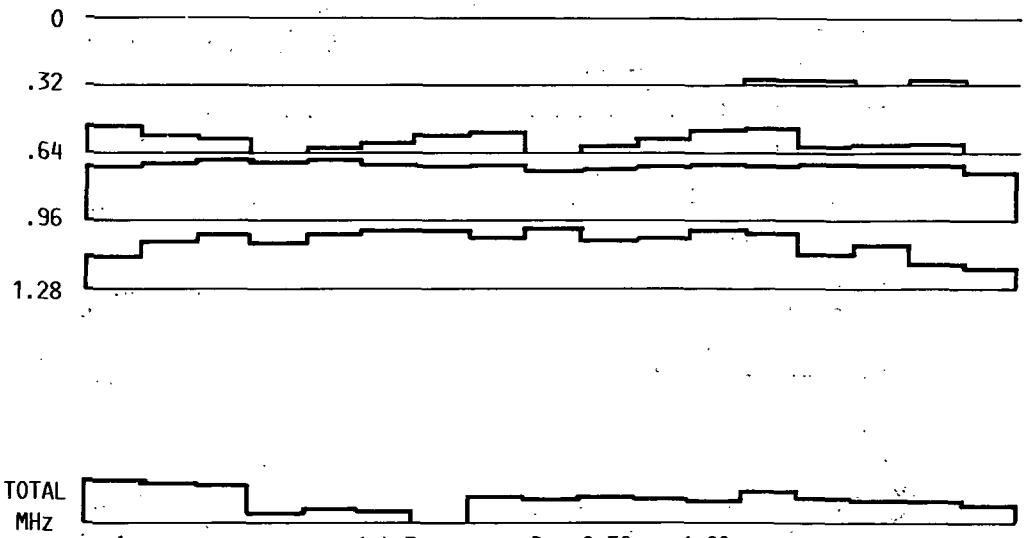

(B) BAR GRAPH R = 0.50 TO 1.00.

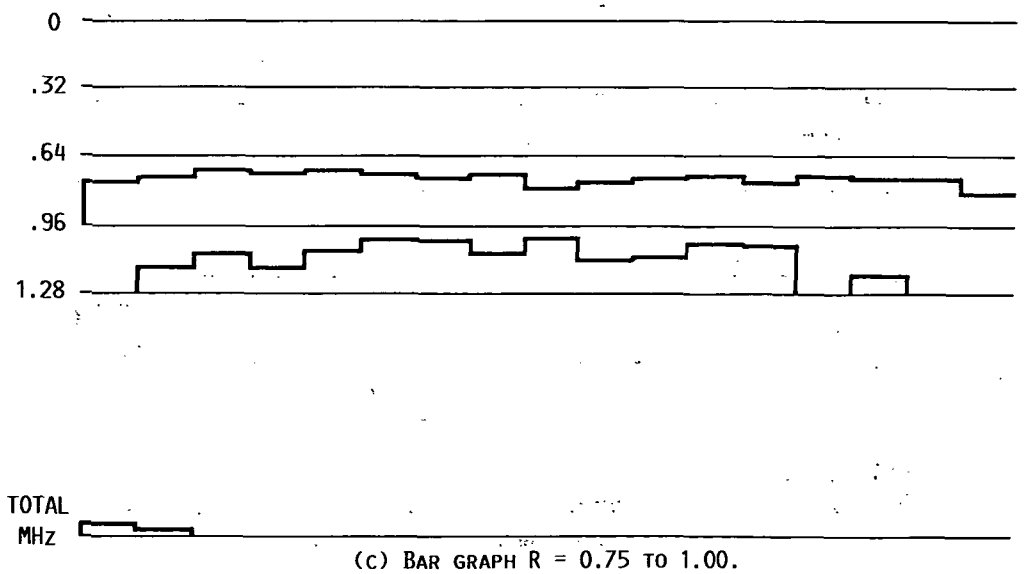

(C) BAR GRAPH R = 0.75 TO 1.00.

FIGURE 14. - LINEAR REGRESSION COEFFICIENTS FOR PARTITIONED STRESS WAVE FACTOR VERSUS INTERLAMINAR SHEAR STRENGTH. SPECIMENS INCLUDED: 8 SELECTED. POSITION OF SWF MEASUREMENT: NO. 7, CONVEX SIDE.

20 µsec PARTITION WIDTH STARTING AT:

	0	1	2	3	4	5	6	7	8	9	10	11	12	13	14	15	16	µsec
0	0.76	0.90	0.67	0.59	0.47	0.33	0.32	0.48	0.55	0.50	0.44	0.54	0.65	0.66	0.60	0.57	0.56	
.32	0.89	0.88	0.84	0.84	0.86	0.82	0.85	0.79	0.83	0.80	0.80	0.81	0.78	0.76	0.76	0.69	0.69	
.64	0.57	0.65	0.59	0.60	0.57	0.57	0.63	0.66	0.66	0.67	0.65	0.65	0.67	0.67	0.66	0.73	0.80	
.96	0.93	0.94	0.94	0.94	0.96	0.94	0.97	0.91	0.93	0.94	0.92	0.92	0.92	0.89	0.84	0.78	0.81	
1.28																		
TOTAL MHz	0.85	0.90	0.89	0.80	0.77	0.69	0.72	0.75	0.81	0.76	0.74	0.76	0.78	0.75	0.70	0.68	0.66	

(A) VALUE OF R.

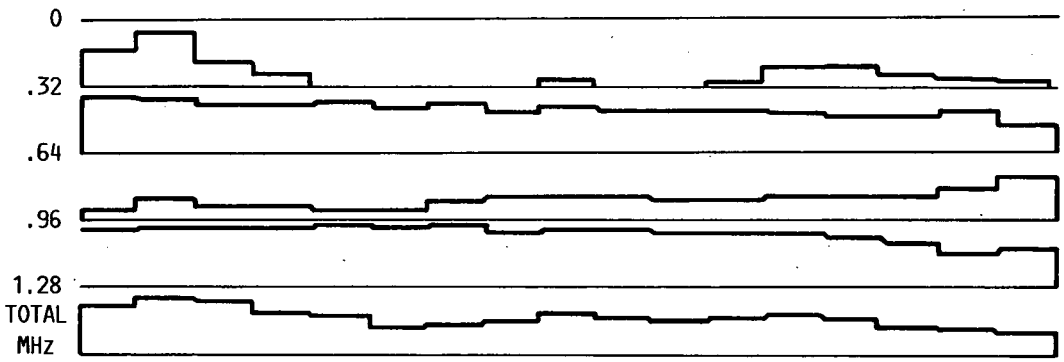

(B) BAR GRAPH R = 0.50 TO 1.00.

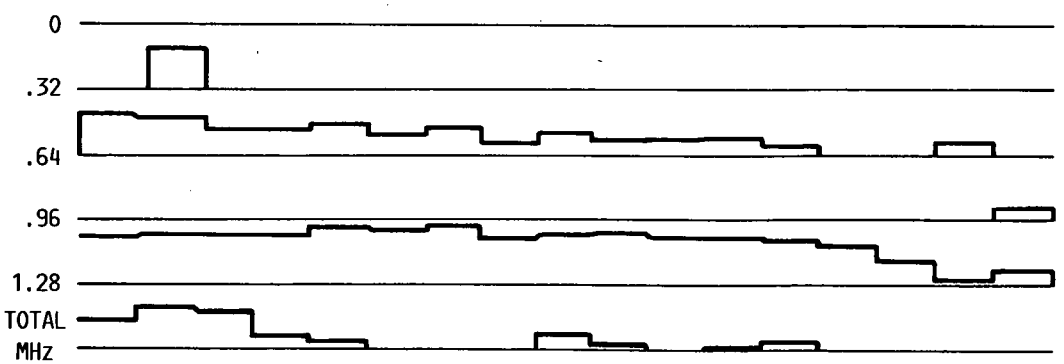

(C) BAR GRAPH R = 0.75 TO 1.00.

FIGURE 15. - LINEAR REGRESSION COEFFICIENTS FOR PARTITIONED STRESS WAVE FACTOR VERSUS INTERLAMINAR SHEAR STRENGTH. SPECIMENS INCLUDED: 8 SELECTED. POSITION OF SWF MEASUREMENT: NO. 7, CONCAVE SIDE.

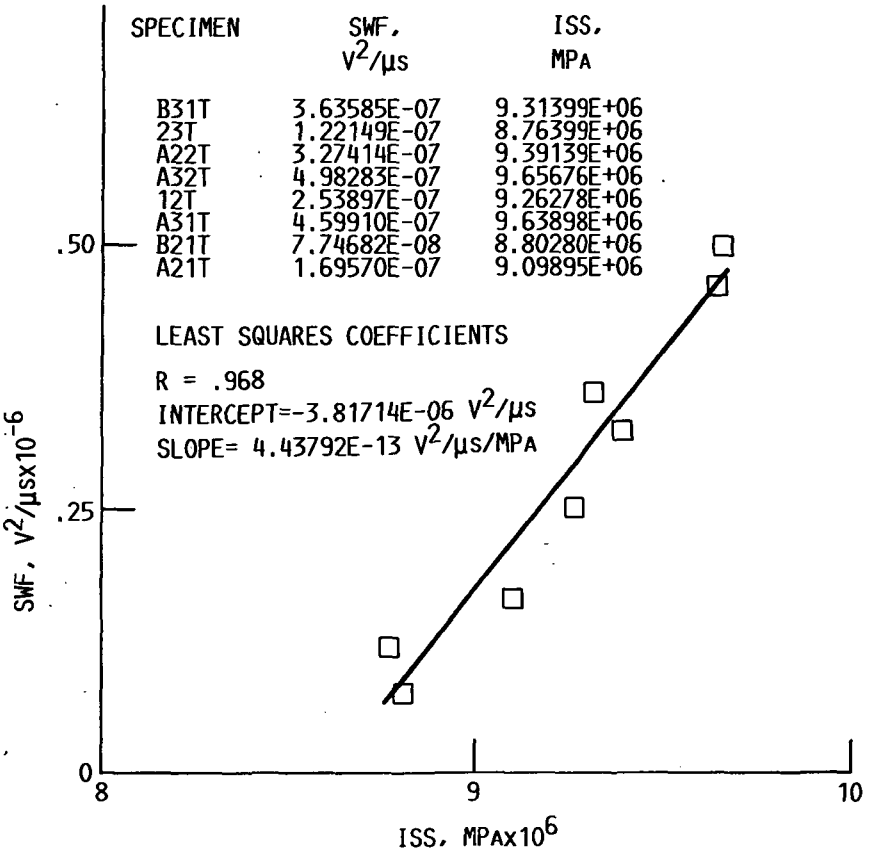

FIGURE 16. - STRESS WAVE FACTOR VERSUS INTERLAMINAR SHEAR STRENGTH WITH LINEAR REGRESSION CURVE. POSITION: 7. CONCAVE SIDE. PARTITION: 6 TO 26 MICROSECONDS AND 0.96 TO 1.28 MHz.

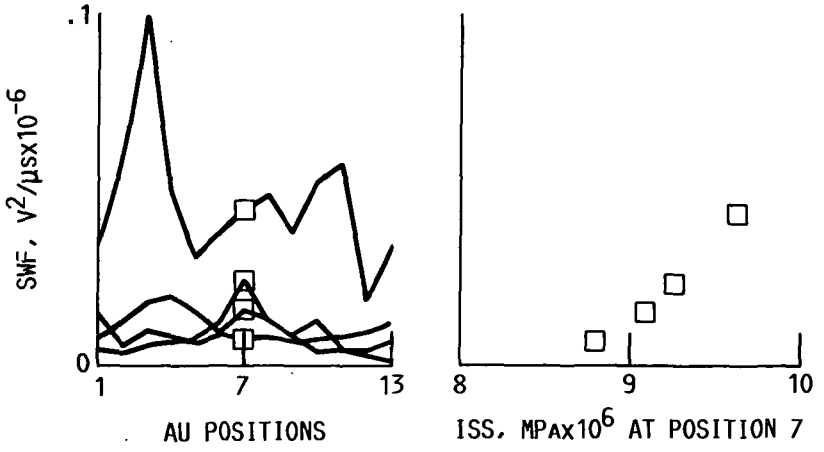

FIGURE 17. - SWF OF FOUR OF THE SPECIMENS AND PARTITION IN FIGURE 15. SWF IS PLOTTED VERSUS POSITION ON SPECIMENS WITH POSITION 7 MARKED WITH SYMBOL. POSITION 7 SWF IS ALSO SHOWN VERSUS ISS.

1. Report No.	2. Government Accession No.	3. Recipient's Catalog No.
NASA TM-88827		

4. Title and Subtitle	5. Report Date
Acousto-ultrasonic Verification of the Strength of Filament Wound Composite Material	6. Performing Organization Code: 506-41-11
7. Author(s): Harold E. Kautz	8. Performing Organization Report No.: E-3201
	10. Work Unit No.
9. Performing Organization Name and Address: National Aeronautics and Space Administration, Lewis Research Center, Cleveland, Ohio 44135	11. Contract or Grant No.
12. Sponsoring Agency Name and Address: National Aeronautics and Space Administration, Washington, D.C. 20546	13. Type of Report and Period Covered: Technical Memorandum
	14. Sponsoring Agency Code

15. Supplementary Notes

Presented at the Pressure Vessel Conference, sponsored by the American Society of Mechanical Engineers, Chicago, Illinois, July 21-24, 1986.

16. Abstract

The concept of acousto-ultrasonic (AU) waveform partitioning was applied to nondestructive evaluation of mechanical properties in filament wound composites (FWC). A series of FWC test specimens were subjected to AU analysis and the results were compared with destructively measured interlaminar shear strengths (ISS). AU stress-wave factor (SWF) measurements gave greater than 90 percent correlation coefficient upon regression against the ISS. This high correlation was achieved by employing the appropriate time and frequency domain partitioning as dictated by wave propagation path analysis. There is indication that different SWF frequency partitions are sensitive to ISS at different depths below the surface.

17. Key Words (Suggested by Author(s))	18. Distribution Statement
Nondestructive testing/evaluation; Ultrasonics; Acousto-ultrasonics; Composites; Interlaminar strength; Stress waves; Frequency spectrum analysis	Unclassified - unlimited STAR Category 38

19. Security Classif. (of this report)	20. Security Classif. (of this page)	21. No. of pages	22. Price*
Unclassified	Unclassified		

*For sale by the National Technical Information Service, Springfield, Virginia 22161

National Aeronautics and
Space Administration

Lewis Research Center
Cleveland, Ohio 44135

SECOND CLASS MAIL

ADDRESS CORRECTION REQUESTED

Postage and Fees Paid
National Aeronautics and
Space Administration
NASA-451

NASA